M.-P. Bacos, J.-M. Dorvaux, S. Landais, O. Lavigne, R. Mévrel, M. Poulain, C. Rio, M.-H. Vidal-Sétif
(Onera)

E-mail: odile.lavigne@onera.fr

10 Years-Activities at Onera on Advanced Thermal Barrier Coatings

Developing thermal barrier coatings operating at higher temperature and/or for very long durations (commercial aircraft applications) is one of the technological and economic challenges for engine manufacturers. This includes the search for (i)low thermal conductivity, high thermal stability and CMAS resistant ceramic top coats, and (ii)alternative low cost bond coats with improved oxidation resistance and chemical compatibility with the substrate. This paper reviews the rationale supporting the choice of new materials for each layer and presents some recommendations to develop more robust and more efficient systems with increased lifetime.

Introduction

Thermal barrier coatings (TBCs) have been used since the 70s to protect metallic parts in the hot sections of gas turbines. TBCs are multilayer systems including a thermal insulating porous ceramic layer, mostly of 8 wt.% yttria partially stabilized zirconia 8YPSZ, deposited on an alumina forming metallic bond coat in contact with the nickel-based superalloy substrate. They are designed to improve engine efficiency by prolonging the component lifetimes and/or increasing gas temperature while reducing emissions and costs. Nevertheless first generation TBCs turned out to be prone to rapid ageing and degradation in service [1]. Demands for advanced thermal barrier systems with enhanced reliability and performance emerged in the early 1990s, especially for applications at higher operating temperatures and/or for very long durations. This paper gives an overview of some activities performed at Onera in this field during the past ten years, with respect to the state-of-the art. It focuses on the development of low thermal conductivity, high thermal stability and CMAS resistant ceramic top coats and alternative low cost bond coats with improved oxidation resistance and chemical compatibility with the substrate.

New Ceramic Coatings

Low thermal conductivity TBCs

Thermal conductivity at 1200°C of the current state-of-the-art 8YPSZ top coat is typically 1.5 to 1.8 $W.m^{-1}.K^{-1}$ for EB-PVD coatings with columnar porosity (blades and vanes applications) and 0.8 to 1.0 $W.m^{-1}.K^{-1}$ for lamellar porosity structured plasma sprayed coatings (combustors and non-rotating or large component applications). Reducing these values to 30-40 % -all other parameters being kept constant- could ensure significant benefits regarding turbine entry temperature, metal substrate temperature, component life duration, cooling rate and specific fuel consumption [2]. Thus increasing the thermal barrier coating insulation capability emerged as a real technical and economic challenge for engine designers and manufacturers and has been widely documented and patented since the end of the 90s [3,4].

The thermal conductivity of a porous layer depends on the intrinsic thermal conductivity of the bulk material, which is linked with its composition and its structure, and on the architecture of the porous structure, i.e. pore volume fraction, geometry and distribution. Thus, lowering the thermal conductivity of the ceramic layer can be achieved by engineering chemical composition and/or coating microstructure.

Influence of chemical composition

Dense zirconia based materials already exhibit low thermal conductivity (2 – 3 $W.m^{-1}.K^{-1}$ at 1200°C) which is governed by phonon-phonon and phonon-point defect interactions. In partially and fully stabilized zirconia systems, the point defects acting as phonon scatter centers are stabilizing substitution ions and associated oxygen vacancies [5]. It has been shown [6] that the thermal conductivity of single crystal yttria doped zirconia at room temperature is a decreasing function of the yttria content (i.e. of the defect concentration) at least for relatively low stabilizer contents. Beyond a composition corresponding approximately to 20YFSZ the thermal conductivity increases again, although more slowly [7]. This latter effect was attributed to a short range ordering of the point defects, in particular of the oxygen vacancies [8].

Further thermal conductivity decrease may be achieved with stabilizers having different atomic mass and/or ionic radius. A semi-empirical model based on solid state physics considerations regarding heat conduction mechanisms in disordered oxide ceramics has been developed [9] for calculating the thermal conductivity of zirconia based materials doped with trivalent and pentavalent metallic ions as a function of composition, defect content and temperature.

Thus, replacing yttrium by different rare earth elements such as Dy, Yb or Sm causes the thermal conductivity of partially and fully stabilized zirconia to decrease. It appears that the distortion effect linked with the difference in ionic radius is predominant over the mass effect. Furthermore it has been shown that additional doping of yttria or other rare earth partially or fully stabilized zirconia with wisely chosen amounts of Nb or Ta can significantly lower the thermal conductivity. This semi-empirical approach served as a guideline for preparing dense zirconia based new materials, showing that significant decrease in thermal conductivity (up to 40%) can be achieved, compared to the standard 8YPSZ [9]. Similar conclusions on multiple doping of zirconia ceramics have been obtained in many publications and patents during the past decade [3,4,10,11].

To go beyond this approach, a more physically based model has been developed with reliable descriptions of the fine microstructure via Monte Carlo simulations and non equilibrium molecular dynamic calculations of the thermal conductivity [8]. This method has first been validated for the yttria-zirconia system. Calculations showed a rather good agreement with experimental data, in particular concerning the trends as a function of temperature and yttria content [12]. In a second approach the molecular dynamic methodology has been successfully applied on more complex structures, such as pyrochlores (rare earth zirconates or hafnates) and perovskites [13]. Resulting calculated thermal conductivities turned out to be in good agreement with calculated values of minimum conductivity [3] and experimental data from the literature [14,15,16]. In particular calculations performed on several perovskite structure candidates led to the selection of the high melting hexagonal ordered BMT – $Ba(Mg_{1/3}Ta_{2/3})O_3$ - which showed a particular low thermal conductivity (1.4 $W.m^{-1}.K^{-1}$ at 1200°C) associated with a high thermal expansion coefficient (9.10^{-6} K^{-1} between 200 and 1200°C). These calculated predictions tallied with published results [17,18] and were confirmed experimentally on dense BMT synthesized through a solid state route [13,19].

Besides this work on dense materials, alternative compositions deposited by plasma spraying, EB-PVD or PE-CVD [Box 1] have been tested within national or international projects [1, 2, 3, 4]: simple binary tetragonal or cubic zirconia based coatings [20,21], ternary zirconia systems [22], ceramics with more complex crystallographic structures like pyrochlores [23],… Thermal conductivity as low as half the thermal conductivity of standard 8YPSZ with similar porosity could be achieved for a given coating process [24].

Influence of porous architecture

Another efficient way to decrease the thermal conductivity of a material is to introduce microstructural defects such as pores, voids, microcracks which constitute obstacles against the through-thickness heat transfer. This approach turned out to be very fruitful in case of plasma sprayed coatings by use of specially designed feedstock powders and/or by control of spray parameters[1]. In the case of EB-PVD or PE-CVD coatings [25] a gain in thermal insulation has also been obtained with particular columnar architectures although smaller than the one achieved with optimized chemical composition[1].

Several methods can be found in the literature which attempt to estimate the thermal conductivity of porous materials as a function of microstructural features. Analytical calculations are mostly derived from the earliest electrical models of Maxwell (1898) and Eucken (1932) and are based on a restricted geometrical description of the porosity. Although these models might be relevant for describing trends in particular materials, the oversimplifying assumptions they rely on, singularly restrict their predictive capacity in the case of more complex interconnected porous structures, such as those observed in EB-PVD or plasma sprayed coatings, even if they have been widely used in the latter case [26].

Numerical approaches involving a representation of the actual microstructure are more promising. Finite element methods[5] turned out to be very costly in terms of meshing and memory storage as far as very small porous features are concerned (inter-lamellar voids in plasma sprayed coatings or intra-columnar porosity in EB-PVD coatings as small as 0.1 μm). An alternative approach based on a finite difference method has been developed at Onera [27] using no meshing but digitized micrographs of real coating cross sections as input for the thermal conductivity calculation [Box 2]. Several applications on thermal barrier coatings -mainly plasma sprayed ones- have illustrated the possibilities of this approach in its 2-dimensionnal (2D) version [28], such as:

- estimating the contribution of each morphological feature to the thermal conductivity and their role in its evolution as a result of heat treatments (sintering), thus providing a guideline for engine manufacturers for designing more efficient coatings with optimized thermal properties
- determining the various thermal conductivity components of an anisotropic coating and assessing the effective thermal conductivity in the case of multiphase or multilayer materials possibly with thermal boundary resistances
- evaluating the thermal conductivity of materials in conditions where experiments may be very difficult to carry out, i.e. at high pressure and/or high temperature.

In order to improve the reliability of the FDM calculation, which depends strongly on the representativeness of the input images of the microstructure, a 3-dimensional (3D) extension of this approach has been developed [Box 2]. Such application to thermal barrier coatings is still difficult due to poor reliable high resolution 3D representations of such coatings although new techniques such as FIB sectioning or nano computer tomography should make it possible in a near future.

---

[1] European project HITS: High Insulation Thermal barrier coating Systems, 4th FWP (1997-2002)

[2] European project TBC+: New Increased Temperature Capability Thermal Barrier Coatings, 5th FWP (2001-2006)

[3] EU-US Project HIPERCOAT: Science of High Performance Multifunctional High Temperature Coatings (2002-2005)

[4] European project TOPPCOAT: TOwards design and Processing of advanced, comPetitive thermal barrier COATing systems 6th FP (2006-2010)

[5] OOF (http://www.ctms.nist.gov/oof): Object Oriented Fine Element Modelling in Materials Science

Box 1 - Plasma Enhanced CVD

Equipment / Principle

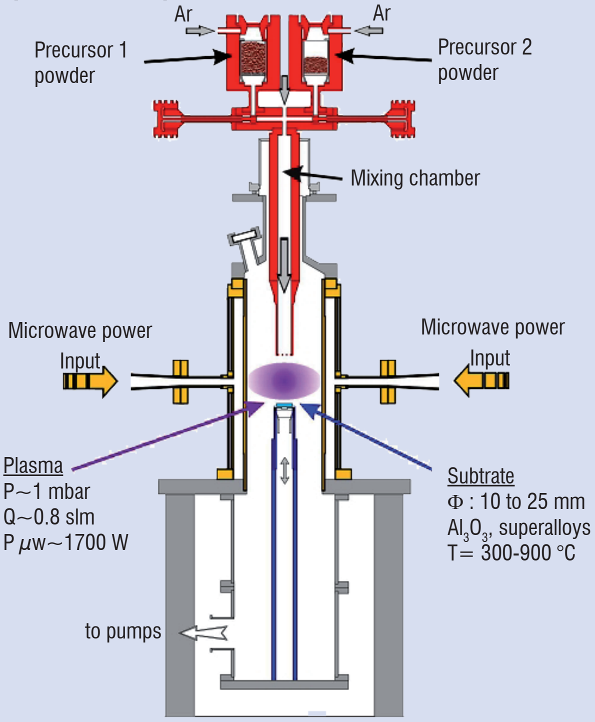

Figure B1-01 – PE-CVD equipment sketch

Equipment characteristics

Gas flow
- coating oxygen stoichiometry
- coating thickness homogeneity

Evaporation or sublimation temperature (100 to 250 °C)
- coating rate (YPSZ: 50 to 250 μm/h)
- coating composition

Deposition temperature (300 to 1000 °C)
- coating porosity (YPSZ: 20 to 50 %)

Precursors (chloride or organo-metallic powders)
- coating composition

Two Onera facilities

Laboratory reactor: coatings on planar substrates (3 cm^2)

Pre-industrial reactor: coatings on turbine blade or vane (50 cm^2)

Coating characteristics

- Columnar structure, similar to EB-PVD
- Complex composition (up to three different oxides), providing available precursors
- Coating on complex shape component (Low line-of-sight process)
- Single or multilayer
- Total cost mostly depends on precursors

Some deposited compositions : 8YPSZ, 20YFSZ, Nd_2O_3 doped zirconia, HfO_2, La,Gd-garnet, alumina,...

Example

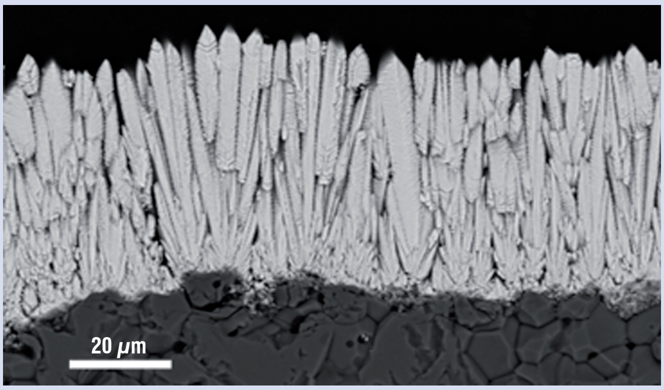

Figure B1-02 – PE-CVD coating microstructure (ZrO_2+12 mol.% Nd_2O_3)

Box 2 - FDM calculation of thermal conductivity

2D calculation («TBCTOOL» code): principle

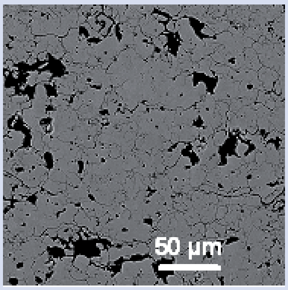

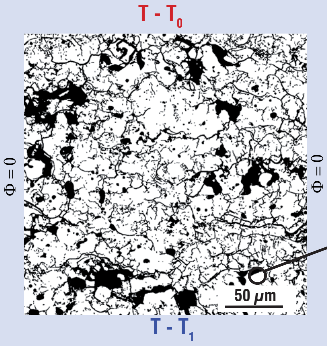

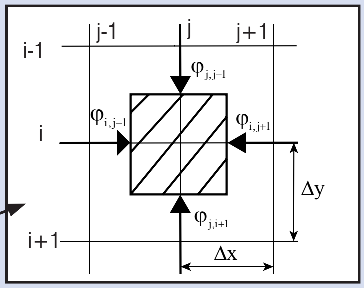

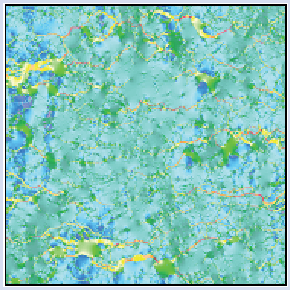

Figure B2-01 – SEM-BSE image of coating cross section (plasma sprayed TBC)

Figure B2-02 – Input data:
- Threshold binary image
- Thermal conductivity (K) of the matrix
- K gas inside the pores

Figure B2-03 – Numerical scheme: resolution of heat equation for each

Figure B2-04 – Output data:
- Effective thermal conductivity tensor
- Temperature, heat flux, thermal gradient maps

Validation: comparison with FEM calculation

Some tests were done on EB-PVD coating morphologies in order to compare the solutions produced by the Onera TBCTOOL FDM-code and the OOF FEM-code developed at NIST [29]. Due to the very large requirement in memory storage the latter approach was not able to compute directly the conductivity of 1024 x 1024 pixels fields and input images had to be decomposed into slices. The two codes gave close results despite the difference in the computational methods and in the method used to handle boundary conditions.

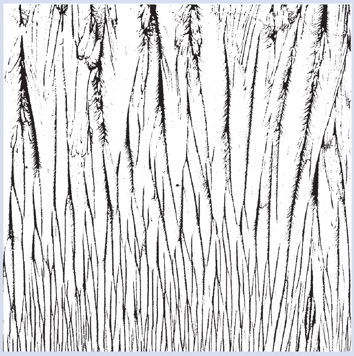

EB-PVD TBC n°	Measured conductivity K $[W.m^{-1}.K^{-1}]$	K -TBCTOOL whole image $[W.m^{-1}.K^{-1}]$	K-OOF 4 vertical slices $[W.m^{-1}.K^{-1}]$	Porosity [%]
1	0.78	0.53	0.59	17
2	0.77	0.52	0.54	22
3	0.61	0.33	0.41	27

Figure B2-05 – Threshold binary image of EB-PVD TBC cross section

Table B2-1 – Measured and calculated (FDM and FEM) thermal conductivity of three different low-thermal conductivity EB-PVD coating microstructures

2D calculation limits:

The reliability of the FDM calculation highly depends on the representativeness of the input images of the microstructure. Plasma sprayed coatings microstructures are generally quite well described with 2D images whereas a 2D approach is of poor relevance for strongly anisotropic EB-PVD coatings. This mainly explains the discrepancies observed between computed and measured values (see table B2-1).

3D calculation (extended "μprop2D")

A more accurate and competitive 2D-code "μprop2D" has been developed using better FDM schemes, different boundary conditions types and an efficient method of storage for the matrix coefficients so that conductivity of fields as large as 5000 x 3400 pixels could be calculated on a 512 Mb computer.

Then the method was extended to three-dimensional fields. The following results have been computed on a 2Gb memory computer (AMD Athlon 1500) with a time cost of 4h50min for phase conductivity ratio of 0.01. The morphological data (512x512x388 voxels) came from the reconstruction of SEM images of serial slices of an EB-PVD coating.

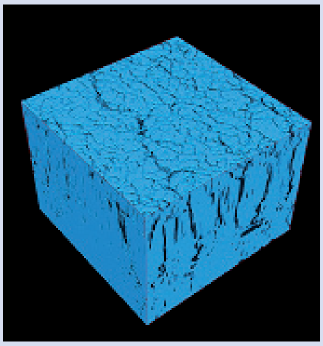

Figure B2-06 – Reconstructed EB-PBD coating morphology

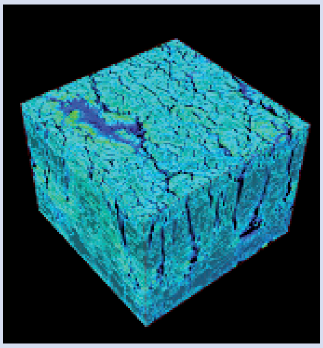

Figure B2-07 – Calculed heat flux

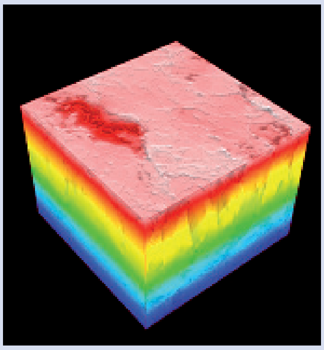

Figure B2-08 – Calculed temperature

$$K = \begin{bmatrix} 0.5365 & -0.01959 & 0.004 \\ -0.01959 & 0.5693 & -0.0003 \\ 0.004 & -0.0003 & 0.8013 \end{bmatrix}$$

Computed thermal conductivity tensor considering periodic boundary conditions and a phase conductivity ratio of 0.01

Some limitations of the 3D calculation

The large volumes of data to be handled may exceed the capacities of an individual ordinary computer. A parallel version of the code should overcome this limitation. Actually it has been demonstrated (EU-US Project HIPERCOAT) that a 1Gvoxels (1024x1024x1024) Laplace problem could be solved on 4x3Gb memory cluster. At the present time a quite common quad core computer with 16Gb of RAM can be used.

Obtaining 3D representations of thermal barrier coatings with suitable resolution and in a reasonable time is still a problem. A 3D volume reconstructed from a series of cross-sections SEM images of an EB-PVD coating has been done once but the method to acquire such images is tricky and time-consuming and can not be widespread. New 3D characterization techniques should provide some solutions.

Additional requirements for the ceramic top coat

TBC long-term stability during service may be of concern, especially with low thermal conductivity coatings as the outer surface temperature is highest or for very long durations, as encountered in commercial aircraft applications. Two main issues are (i) possible phase transformations and (ii) sintering resulting in reduced thermal insulation capability and strain compliance, with TBC system degradation as a consequence [1].

Some low thermal conductivity compositions previously mentioned such as fully stabilized zirconia or zirconates allow the first issue to be avoided. However most of them have to be used as outer layer deposited on an inner layer of 8YPSZ [6, 7]. Actually it is now well established although not yet entirely explained [30] that the longest lifetimes of TBC systems are obtained with 8YPSZ or at least with non transformable t' structured compositions.

Densification of TBCs is a complex phenomenon on account of the constraint imposed by the metallic substrate and the external applied thermomechanical conditions. It depends on the coating microstructure and to a minor extent on its composition. Surface energy is the driving force for sintering and the dominant mechanism at operating temperatures ($<$ 1300 °C) is likely to be surface diffusion. An original method [31] has been adapted at Onera [19] for determining surface diffusion coefficients from grain boundary thermal grooving estimated from atomic force microscopy experiments (Box 3). It appears that some new low thermal conductivity compositions (particularly in the rare earth–zirconia system) are more sintering resistant than standard 8YPSZ.

Currently most research activities regarding top coat compositions are related to an even more critical issue for TBC lifetime, i.e. TBC degradation by CMAS attack.

[6] European project HITS: High Insulation Thermal barrier coating Systems
[7] European project TBC+: New Increased Temperature Capability Thermal Barrier Coatings

Box 3 - Surface diffusion coefficient estimation from AFM profile of thermally grooved grain boundaries

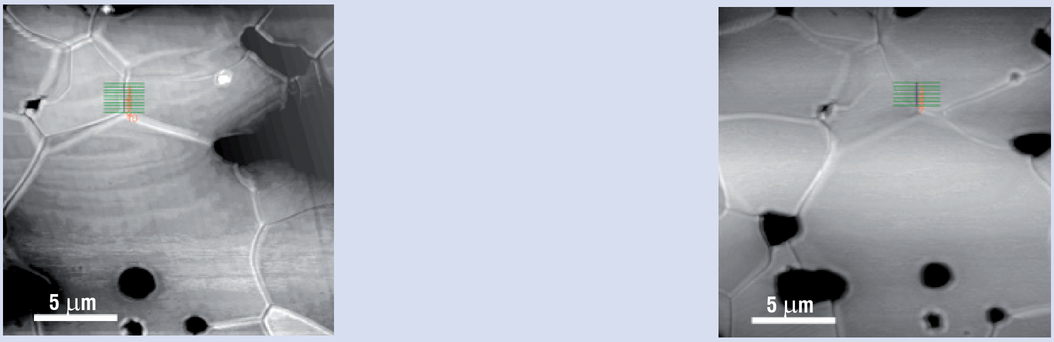

Figure B3-01 – AFM images of the same zone in dense 20YFSZ after annealing at 1300 °C for 12 hours (left) and 96 hours (right)

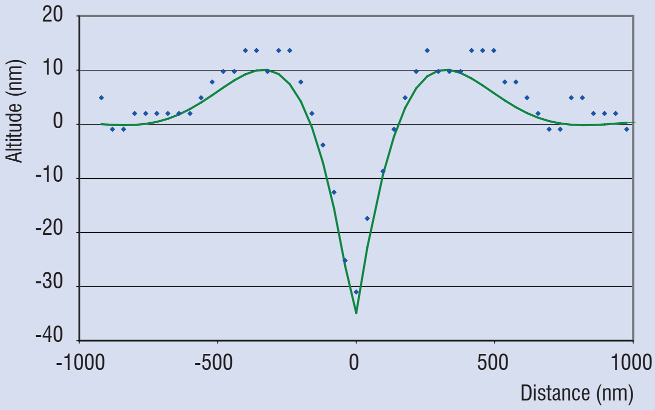

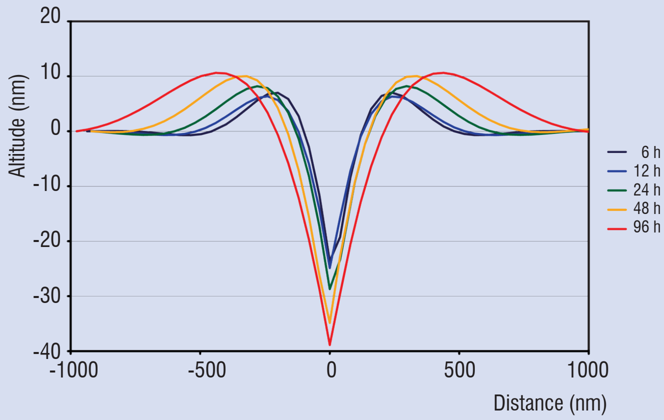

Figure B3-02 –
♦ Mean experimental profile of a given grain boundary extracted from AFM image at given (Temperature, time)
— Fit (Matlab) with Mullins equation for surface diffusion [W.W. Mullins – *Theory of thermal grooving*. J. Appl. Phys., 28 (1957) 333-339]

Figure B3-03 – Evolution of the profile (fitted) of the same grain boundary for different annealing times at 1300 °C.

→ **output data**: surface diffusion coefficient and grain boundary equilibrium angle at given (T,t)

→ **output data**: surface diffusion coefficient as a function of temperature (activation energy of surface diffusion)

Some experimental surface diffusion coefficients obtained at 1300 °C [$m^2.s^{-1}$]: 4.10^{-15} for 20YPSZ, 4.10^{-16} for dysprosia fully stabilized zirconia and 4.10^{-14} for hexagonal ordered BMT – $Ba(Mg_{1/3}Ta_{2/3})O_3$ perovskite [19].

CMAS resistant coatings

Investigations on blades removed from service in the early 2000s showed that thermal barrier coatings are susceptible to degradation by molten calcium-magnesium-alumino-silicates (CMAS) resulting from the ingestion of siliceous mineral debris (dust, sand, ash) contained in the hot gases arriving in the turbine. Since then various solutions to the problem of CMAS degradation have been attempted. All of them consisted in depositing a protective coating on the surface of thermal barrier coating. Early solutions, most of them published in patents, were divided into three types: impermeable, sacrificial or non-wetting coatings [32,33,34]:

• The impermeable barrier is able to inhibit the infiltration of molten CMAS. It consists in a dense, non-cracked and non porous ceramic or metal outer layer [33]. Examples of such coatings are Pd, Pd-Ag, Pt, SiC, SiO_2, Sc_2O_3, SiO_xC_y, Ta_2O_5, $MgAl_2O_4$, and $CaZrO_3$.

• The sacrificial coating reacts with CMAS to increase the melting temperature or viscosity of the contaminants thereby inhibiting infiltration [32,33,35,36,37]. Examples are silica, scandia, alumina, chromia, magnesia or calcia layers or alumina particles embedded in a silica matrix.

• The non-wetting outer layer minimizes contact between underlying layers and the molten contaminants. Non-wetting coatings mentioned as especially effective are noble metals as Pd, Pt, Pd-Ag alloy, AlN, BN, SiC, $MoSi_2$, SiO_2, $ZrSiO_4$, SiOC [34].

Other solutions, such as an aluminum phosphate layer [38] or Ta_2O_5 layer [39] are also proposed in the patent literature. Though there are a large number of identified protective coating compositions, none of them seems to be effective enough, especially with increasing operating temperatures.

More recently, as a result of studies on low thermal conductivity TBCs (see § Low thermal conductivity TBCs) a solution has been patented consisting in a two layer system [40]. The inner layer is a stabilized zirconia layer such as 8YPSZ and the outer layer, a CMAS resistant zirconia based material doped with an effective amount of rare earth oxides such as Gd, La, Eu, Sm, Nd-oxides. The base material can also be a zirconate $X_2Zr_2O_7$ (pyrochlore structure) where X is a rare earth element. In the open literature, Krämer [41] has shown that a layer of gadolinium zirconate $Gd_2Zr_2O_7$ is effective to arrest CMAS infiltration. Indeed, the high temperature reaction between CMAS and gadolinium zirconate produces a dense crystalline layer consisting of an apatite phase $Gd_8Ca_2(SiO_4)_6O_2$ and fluorite ZrO_2 (with Gd and Ca in solid solution) which rapidly fills the intercolumnar gaps of EB-PVD top coat.

The studies conducted at Onera have investigated the interaction between CMAS and a ceramic from the ZrO_2-Nd_2O_3 system. The experimental approach adopted was to simulate the CMAS corrosion at laboratory scale, under controlled conditions, using a model synthetic CMAS. Dense materials have been used or EB-PVD coatings deposited on an alumina substrate. Some results are presented below.

Synthetic CMAS interaction with standard 8YPSZ EB-PVD coatings

The first work has consisted in trying to reproduce, in laboratory, the interaction observed between CMAS and 8YPSZ TBC on a high pressure turbine blade removed from service [1]. The model CMAS composition 61.5SiO_2-15Al_2O_3-23.5CaO (wt.%) is the lowest melting eutectic (1170 °C) in the ternary (CaO-Al_2O_3-SiO_2) system. It has been selected on the base of a melting temperature compatible with real thermal barrier surface temperature (≈1200 °C). In a first approach, the effect of Fe or Ti has not been taken into account as Krämer did [42] whose synthetic CMAS composition is 33.2CaO-6.5MgO-11.8Al_2O_3-48.5SiO_2 (wt.%).

The CMAS was prepared by mixing fine powders of the individual oxides and carbonates in de-ionized water, then drying and smelting in a Pt crucible at 1250 °C during 20 hours under air to achieve a homogenized melt. After quenching in water, a transparent and homogeneous glass was obtained which was then crushed in a mortar/pestle for obtaining fine glass powders. In order to study CMAS/TBC interaction, the glass-CMAS powders were deposited at the surface of the TBC specimens (30 mg/cm^2) and the CMAS-covered specimens were heat-treated at 1200 °C in air for 4 hours and finally quenched in air.

Figure 1 shows a cross-section SEM image of the TBC specimen which has been exposed to the model CMAS at 1200 °C for 4 hours and the corresponding elemental maps of Ca (Kα line). It can be seen that model CMAS completely infiltrates the TBC intercolumnar gaps down to the alumina substrate.

A higher magnification of the upper interaction zone between model CMAS and TBC (figure 2) shows that TBC columns have been attacked by CMAS especially in the periphery (column tips and feathery porosity) resulting in their morphology degradation. Two new crystalline phases are observed at the interface between TBC and CMAS and in the intercolumnar gaps. These new phases have been identified by XRD and EBSD respectively as $Ca_2ZrSi_4O_{12}$ and $CaAl_2Si_2O_8$ (needle-like morphology anorthite). Moreover EDS analysis reveals that the CMAS is enriched with minor amounts (≤ 1 atom %) of Zr and Y. The enrichment is still observed far from the TBC/CMAS interface. This analysis is consistent with the hypothesis of a dissolution solution of the TBC in the molten CMAS.

From these results, it can be seen that the model system gives very good replication of the CMAS corrosion observed on ex-service blades in terms of thermochemical interaction: TBC infiltration, TBC dissolution in the CMAS melt and formation of new crystalline phases.

Figure 1 – 8YPSZ EB-PVD top coat infiltrated by synthetic CMAS: SEM image (top) and corresponding elemental map of Ca (Kα line) (bottom).

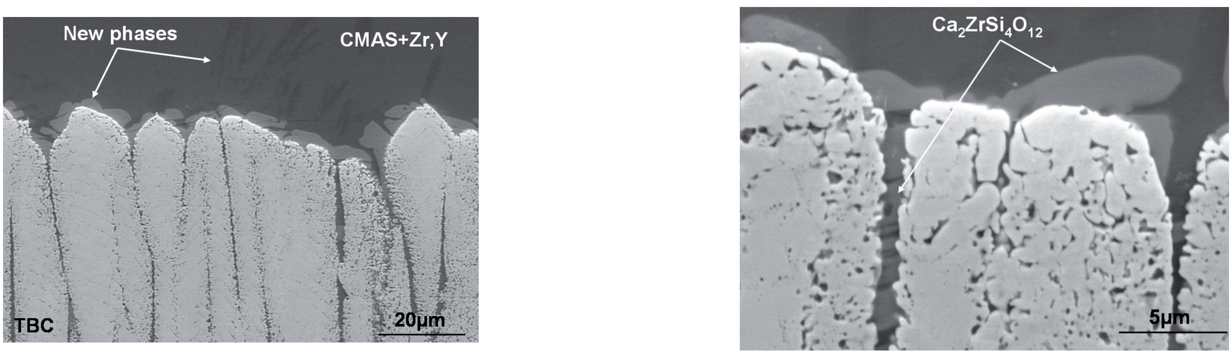

Figure 2 – Reaction zone between synthetic CMAS and TBC after 4 hours at 1200 °C (SEM-BSE image).

Synthetic CMAS interaction with dense ceramics

In a second part, dense ceramic materials have been prepared from pre-alloyed powders by cold isostatic pressing followed by high temperature densification. Two compositions where chosen: ZrO_2+12 mol.% Nd_2O_3 and $Nd_2Zr_2O_7$ (pyrochlore structure) in order to test their resistance to CMAS infiltration. Dense ZrO_2+10 mol.% Y_2O_3 was also prepared as a reference for the ZrO_2-Y_2O_3 system. This composition has been preferred to standard ZrO_2+4.5 mol. % (or 8 wt. %) Y_2O_3 as it allows a unique cubic stable phase whatever the heat treatment applied.

After interaction of the yttria doped zirconia dense specimen with the synthetic CMAS at 1200 °C for 4 hours it appears that the CMAS penetration into the dense ceramic is limited to a few micrometers (figure 3). The top region of the ceramic is attacked resulting in the dissolution of yttria doped zirconia into the CMAS associated with the formation of the crystalline phase $Ca_2ZrSi_4O_{12}$. EDS semi-quantitative analysis reveals that the attacked ceramic surface (figure 3 - right) has a lower ratio Y/Zr than the bulk, indicating that a depletion of yttria took place during the interaction of ZrO_2+10 mol.% Y_2O_3 with CMAS. Thus the result of the interaction between CMAS and the dense ceramic is the same as for 8YPSZ EB-PVD coating.

Synthetic CMAS interaction with ZrO_2+12 mol.% Nd_2O_3 and $Nd_2Zr_2O_7$ at 1200 °C for 1 hour presents some similarities with the one observed with ZrO_2+10 mol.% Y_2O_3, i.e. dissolution of the ceramic in the CMAS, formation of $Ca_2ZrSi_4O_{12}$ in the ceramic top region and depletion of Nd_2O_3 in the attacked ceramic. But a major difference is observed. A dense layer appears (figure 4) between the ceramic grains depleted in Nd_2O_3 and the bulk ceramic. EDS analysis reveals that this layer is mainly constituted of (Zr, Nd, Ca, Si) oxide, suggesting that it is also a reaction product between molten CMAS and the ceramic.

The thickness of this reaction layer increases with the duration of the heat-treatment as seen on figure 5 left for a 25 hours treatment at 1200 °C. At a higher magnification (figure 5 right), the observation of different contrasts in BSE imaging mode indicates that the dense reaction layer is constituted of two interconnected phases. Due to the small size of these phases XRD and transmission electron microscopy should be performed in further work in order to determine the dense layer composition.

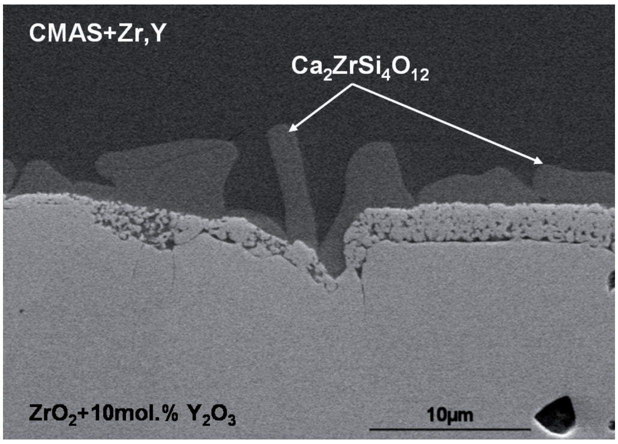

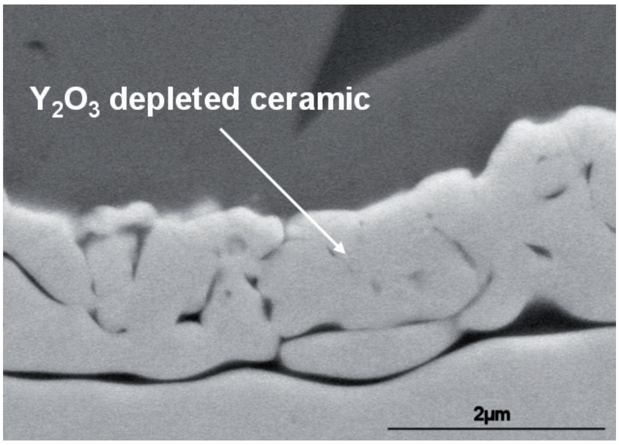

Figure 3 – Reaction zone between synthetic CMAS and dense ZrO_2+10 mol.% Y_2O_3 after 4 hours at 1200 °C; cross-section SEM micrographs (overview (left), detail (right)).

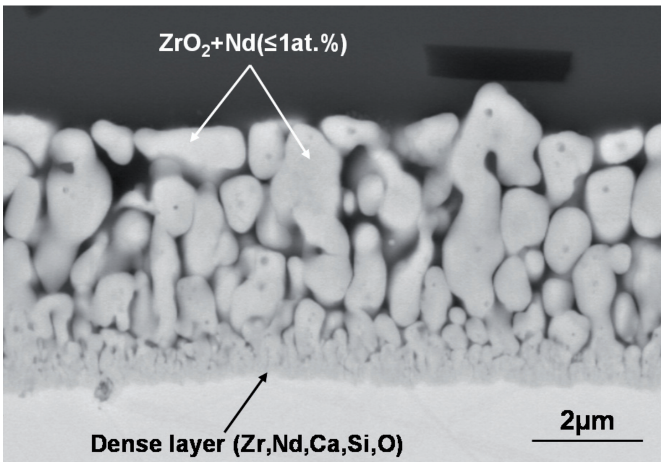

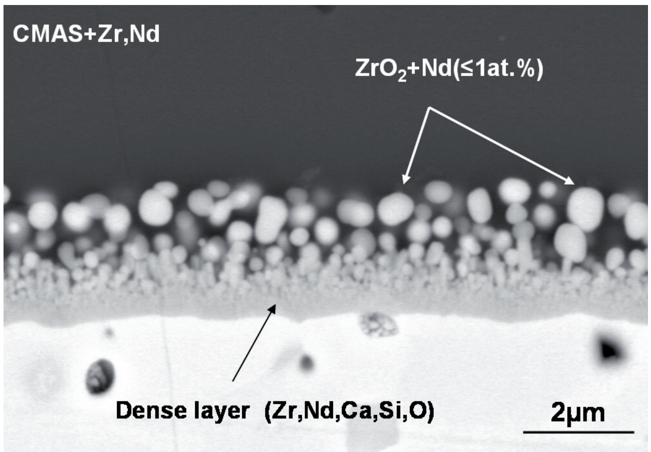

Figure 4 – Reaction zone between synthetic CMAS and dense ceramic after 1 hour at 1200 °C: ZrO_2+12 mol.% Nd_2O_3 (left), $Nd_2Zr_2O_7$ (right).

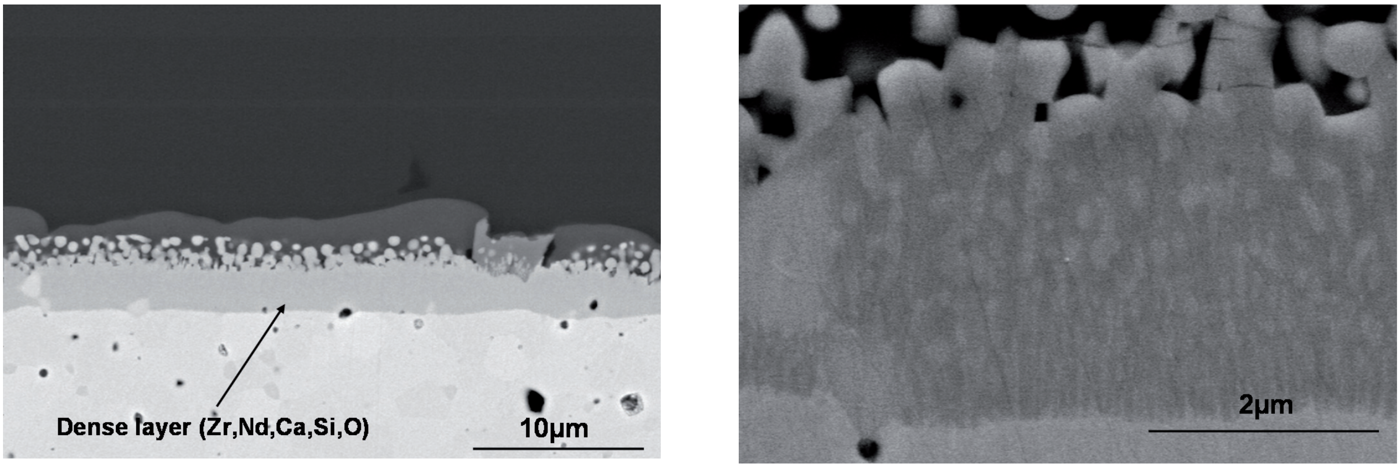

Figure 5 – Reaction zone between synthetic CMAS and $Nd_2Zr_2O_7$ after 25 hours at 1200 °C: overview (left), higher magnification (right).

Synthetic CMAS interaction with a new composition EB-PVD coating

Finally, the thermochemical interaction between a $(La,Nd)_2Zr_2O_7$ EB-PVD coating[8] and the model CMAS has been investigated. After 1 hour at 1200 °C (figure 6 left), the microstructure of the reaction zone between CMAS and ceramic is quite different from the one observed with 8YPSZ EB-PVD coating and very similar to the one obtained with dense $Nd_2Zr_2O_7$. The great difference with 8YPSZ EB-PVD coating is that the model CMAS infiltrated the intracolumnar porosity and the intercolumnar gaps only to a depth $\leq 20\mu m$ below the original $(La,Nd)_2Zr_2O_7$ surface. No evidence of CMAS was found in the rest of the ceramic. Moreover the result of the interaction between the infiltrated CMAS and the ceramic is a dense reaction layer, similar to that observed with the dense $Nd_2Zr_2O_7$ ceramic. EDS analysis reveals that this layer is mainly constituted of (Zr, La, Nd, Ca, Si) oxide. These results suggest that this dense reaction layer, by rapidly filling the ceramic intercolumnar gaps, is responsible for the CMAS infiltration arrest. The same inhibition of CMAS infiltration is still observed after 16 hours at 1200 °C (figure 6 right). These results are in agreement with those obtained by Krämer [41] with the gadolinium zirconate $Gd_2Zr_2O_7$.

As a summary, this work has shown that it is possible to reproduce in laboratory, using a synthetic CMAS, the CMAS corrosion observed on the TBC of a high pressure turbine blade removed from service. The use of dense ceramics in order to test TBC compositions resistant to CMAS has also been validated. Concerning prevention of CMAS infiltration, it seems that ZrO_2+12 mol.% Nd_2O_3 and $Nd_2Zr_2O_7$ could be effective to mitigate the CMAS penetration by the rapid formation of a dense reaction layer in the intercolumnar gaps and the intracolumnar porosity of a EB-PVD TBC. Future work will be devoted to elaborate PE-CVD columnar zirconia coatings containing different amounts of Nd_2O_3 (including the zirconate $Nd_2Zr_2O_7$) in order to confirm their ability to arrest CMAS infiltration. Other rare earth doped zirconia coatings will be tried, first using dense ceramics, then PE-CVD coatings, in order to compare their behavior and to select the most effective composition for the mitigation of CMAS infiltration.

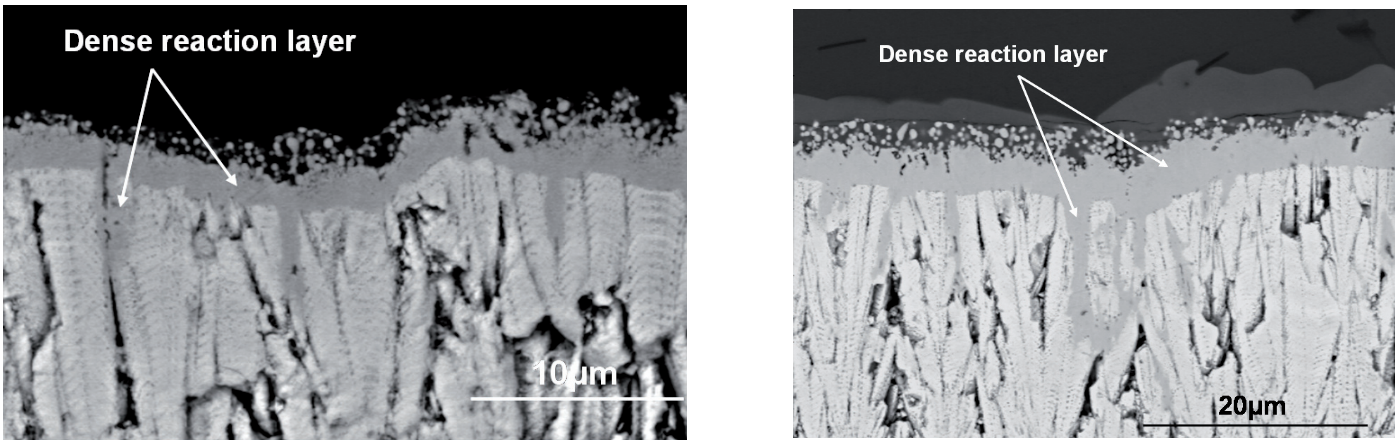

Figure 6 – Reaction zone between synthetic CMAS and $(La,Nd)_2Zr_2O_7$ EB-PVD coating after 1 hour at 1200 °C (left), after 16 hours at 1200 °C (right).

[9] By courtesy of the German Aerospace Center (DLR) – Cologne, within the EU project TBC+ [23]

Alternative bond coats

The search for alternative bond coats to standard platinum modified aluminide is motivated by :

- increasing the adherence of the thermally grown protective alumina scale,
- reducing interdiffusion phenomena between the bond coat and the substrate,
- avoiding phase transitions such as martensite formation,
- increasing creep resistance, in order to minimize surface rumpling and consequently extend the system lifetime,
- reducing the costs.

Zr-doped nickel aluminide

As the addition of reactive elements can have a significant effect on the oxidation behavior of alumina-forming alloys [43], a thermochemical Zr-doping process was developed at Onera [44,45] in order to design Zr-doped NiAl as a bond coat in TBC systems. This non-directional process is well suited for the complex shapes of turbines blades. Moreover there is no need for an electrolytic stage and additionally the use of zirconium instead of platinum decreases the cost of the process.

In this alternative process, zirconium is provided by the $ZrOCl_2,8H_2O$ activator (Box 4). The process leads to the co-deposition of Al and Zr on the nickel-base superalloy. Glow discharge mass spectroscopy (GDMS) profile and multi-spectral X-ray maps indicate that zirconium is located far below the coating surface, at the interface between the β–NiAl coating and the interdiffusion zone (figure 7). Total zirconium concentration (reported to the coating volume) may be evaluated to around 400 at. ppm. The zirconium peak localization at the interface indicates that Zr deposition occurs at the beginning of the vapor phase aluminizing deposition process in agreement with the thermodynamic analysis (HSC Chemistry®). Indeed results from these calculations suggest that Zr deposition mainly occurs at low temperatures (~600 °C). At higher temperatures (~1100 °C) deposition of Al prevails.

Cyclic and isothermal oxidation tests performed at 1100°C showed that adding hundreds of atomic ppm of Zr reactive element in the nickel aluminide improves the adhesion of the alumina scale on the NiAl bond coat [46]. Actually NiAl(Zr) coatings deposited on AM1[9] nickel-based single crystal superalloy presents an oxidation resistance much higher than that of undoped NiAl and comparable to that of NiPtAl coating (Figure 8). The spalled areas revealed the presence of numerous cavities at the metal/oxide interface on AM1/NiAl sample whereas such cavities were never observed on AM1/NiAl(Zr) sample. This absence of voiding in the presence of zirconium is expected to improve thermally grown alumina adhesion on the nickel aluminid.

Isothermal oxidation tests show also that the transient regime of θ-alumina growth lasts shorter with zirconium. Zirconium essentially modifies the transition between the two regimes θ and α but it does not modify the stationary regime of α-alumina growth. However it clearly influences the initial stages of oxide growth and accelerates the transition between the transient and the stationary regimes.

Specific studies using ToF-SIMS experiments show that zirconium, initially located at the interface between the β–NiAl coating and the interdiffusion zone, migrates during oxidation towards the surface leading to a homogeneous depth distribution of zirconium within the whole oxide layer. Zirconium inhibits the formation of cavities at the coating/oxide interface and this could explain the improved spalling resistance observed during cyclic oxidations. This absence of cavities could be due to a shorter transient oxidation, characterized by cationic growth, for NiAl(Zr) coatings, that would prevent cavities growth.

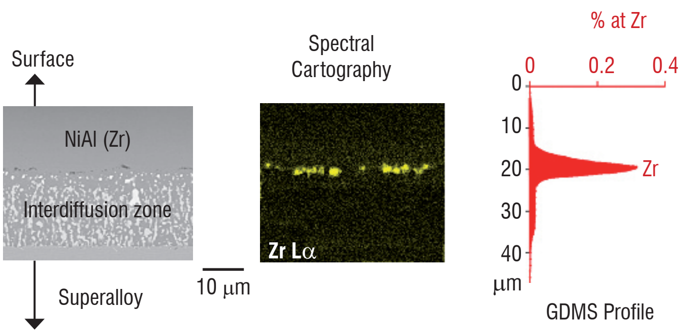

Figure 7 - Zr distribution through alternative Zr-doped aluminide bond coat.

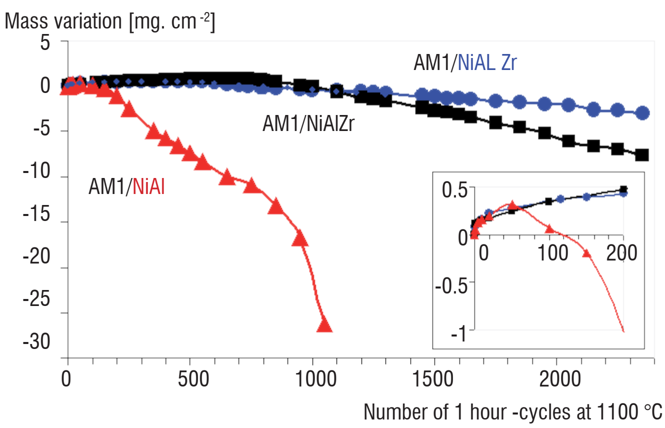

Figure 8 - Cyclic oxidation resistance of different nickel aluminide coatings deposited on AM1 nickel-based single crystal superalloy [47].

[9] AM1 composition [wt. %] : Ni base, 6.5 Co, 7.8 Cr, 2 Mo, 5.7 W, 5.2 Al, 1.1 Ti, 7.9 Ta

Box 4 - Zirconium-doped aluminization

The components to be coated are located in a sealed or semi-sealed retort above a mixture composed of a low aluminum activity cement (Al 30 wt.% Cr 70 wt.%) and a small percentage (from 0.1 to 0.5 wt.%) of a zirconium precursor ($ZrOCl_2$, 8 H_2O) [44,45]. The entire apparatus is placed inside a furnace and heated in a hydrogen atmosphere at high temperature. The duration of the treatment depends on the temperature.

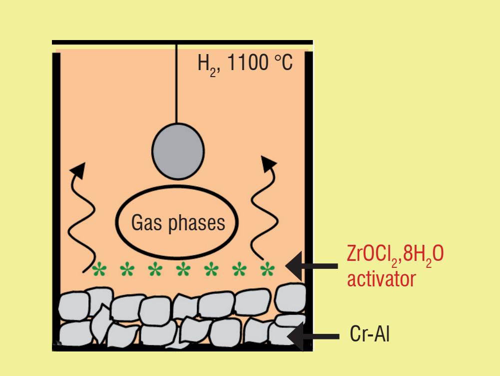

Gas-gas reactions

$ZrOCl_2 + ½\,H_2O \rightarrow ½\,Zr_2O_3Cl_2 + HCl_{(g)}$

$Zr_2O_3Cl_2 \rightarrow ½\,ZrCl_{4(g)} + {}^3/_2\,ZrO_2$ zirconium chloride formation

$Al + HCl_{(g)} \rightarrow AlCl_{(g)} + ½\,H_{2(g)}$ aluminum chloride formation

$AlCl_{3(g)} + 2\,Al \rightarrow 3\,AlCl_{(g)}$

Gas-surface reactions

$AlCl_{(g)}$ + surface $\rightarrow {}^2/_3\,Al + {}^1/_3\,AlCl_{3(g)}$ aluminum deposit

$ZrCl_{4(g)} + 2\,AlCl_{(g)}$ + surface $\rightarrow 2\,AlCl_{3(g)} + Zr$ zirconium deposit

Application of NiAl(Zr) as a TBC bond coat

As mentioned above, the NiAl(Zr) coating is as suitable as the NiPtAl one, when considering cyclic oxidation of aluminized AM1 single crystal superalloy. Consequently, both the standard system AM1/NiPtAl/8YPSZ EB-PVD and the alternative AM1/NiAl(Zr)/8YPSZ EB-PVD one have been studied at Onera [47]. Both systems turned out to have quite similar lifetime although the critical microstructural degradations were found to be different (figure 9). The main mechanisms responsible for the standard TBC system failure are rumpling (increasing interfacial roughness induced by out-of-plane stresses) and formation of large cavities related to the oxidation of the bond coat. As a result local decohesions cleavages arise and interfacial cracks propagate along the TGO/top coat or bond coat interface, and possibly through the TGO itself. On the contrary, no interfacial cavities are detected in the case of the NiAl(Zr) bond coat, and its topographical evolution is appreciably less marked so that the top coat and the TGO spall off together. The less pronounced bond coat deformation is probably due to an enhanced yield stress in the case of Zr-doped nickel aluminide and a low propensity towards martensite NiAl (L10) phase formation. Besides, because the TGO/NiAl(Zr) bond coat interface remains rather smooth, the residual in-plane compressive stress level within the TGO is about 1 GPa higher compared to the standard case [47], which is consistent with the well known effect for Zr to increase the creep strength of alumina.

As a conclusion, the NiAl(Zr) bond coat developed at Onera seems to be a good candidate for less expensive thermal barrier coating systems with operational performance comparable to that obtained with NiPtAl bond coat standard system.

Diffusion barriers

In thermal barrier systems exposed at high temperature interdiffusion phenomena occur between the Ni-base superalloy and the nickel aluminide protective coating, which can have fatal consequences for the life duration of the system. Firstly, interdiffusion increases the extent of Al depletion in the coating, which leads to the acceleration of the β – NiAl $\rightarrow \gamma'$-Ni_3Al transformation and to the formation of non-protective oxide scales. Secondly, particular elements from the superalloy diffuse through the aluminide bond coat up to the thermally grown oxide and some have detrimental effects on the oxide scale adhesion. Finally, for coated third or fourth generation Ni-based superalloys, interdiffusion may lead to the formation of detrimental and fast growing secondary reaction zones (SRZ) [48]. In these SRZ, discontinuous precipitation transforms the single crystal γ/γ' superalloy into a weaker polycrystal composed of γ and TCP phases (σ, μ or P) in a γ' matrix. These zones may degrade the mechanical properties of the system by reducing its load bearing section.

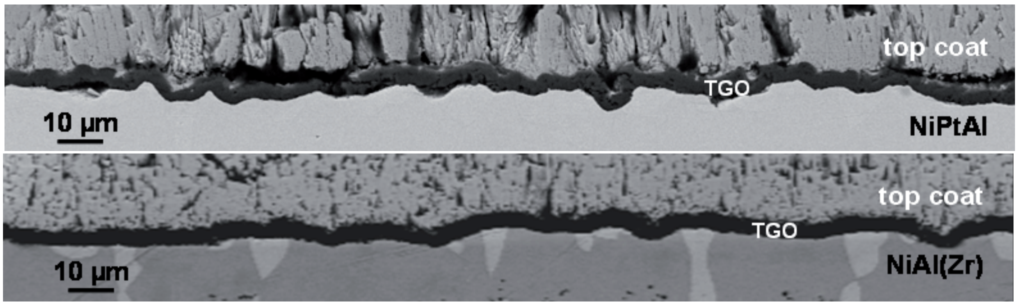

Figure 9 - Interfacial topography after 50 1h-cycles at 1100 °C (AM1/NiPtAl/8YPSZ and AM1/NiAl(Zr)/8YPSZ systems)

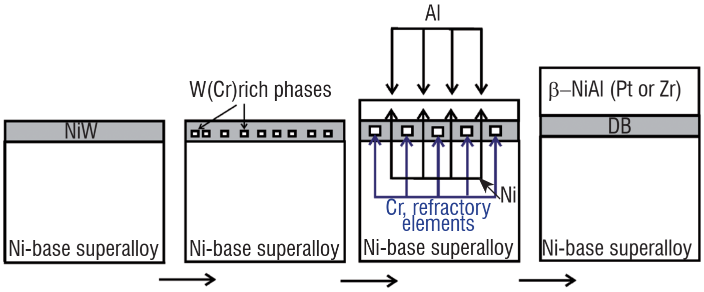

Figure 10 - Principle of a NiW(Cr) diffusion barrier formation after ref [53]

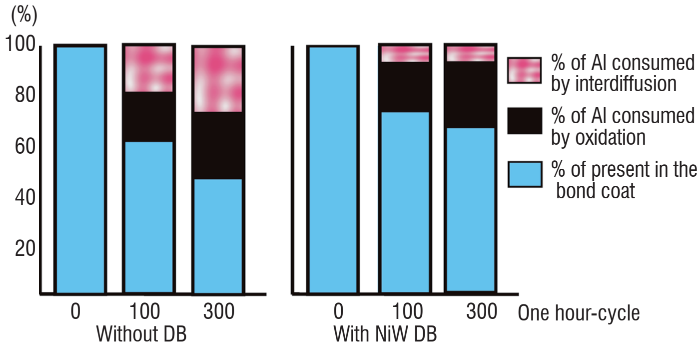

Figure 11 - Efficiency of the diffusion barrier (nickel based superalloy MC-NG[10]/simpleDB/NiPtAl system). Repartition of Al content after oxidation at 1100°C (one hour-cycle); after ref [55].

To limit interdiffusion phenomena between the Ni-based superalloy and its protective coating, some authors have introduced diffusion barriers (DB) [49,50]. Onera has developed [51] such diffusion barriers, which were based on a Ni-W electrolytic coating and composed of a dense precipitation of α-W phases after a thermal treatment under vacuum (simple DB) [52,53] or a vapor phase chromization (Cr enriched DB) [55]. These diffusion barriers have been tested under a classical nickel aluminide coating (Pt modified or Zr doped) (figure 10).

Chemical composition measurements (with EDS spectral maps) coupled with the "p-Kp" modeling [54] of the cyclic oxidation kinetics, and the development of the model "p-Kp-β" at Onera [55] have permitted study of the efficiency of the diffusion barrier as a function of its composition and its ageing at high temperature (figure 11). Isothermal thermogravimetric analysis showed that both as-processed systems without and with NiW diffusion barrier (but without any thermal barrier coating) exhibit similar oxidation kinetics and final mass gains [52].

Finally it has been proved [53] that diffusion barrier modifies the SRZ initiation but not their propagation kinetic, which only depends on the superalloy local composition.

Conclusion

The strong demand from engine manufacturers for improving turbine performance at higher temperature and/or for very long durations has led since the end of the 90s to the development of advanced thermal barrier systems. Onera activities in this field have concerned materials, mechanical and modeling aspects. New compositions and microstructures for a low thermal conductivity, high thermal stability ceramic top coat have been proposed on the basis of thermal conductivity calculations and modeling. Today the search for protective coatings against environment and especially CMAS attack is a priority. Moreover alternative low cost bond coats with improved oxidation resistance and chemical compatibility with the substrate have been developed. Further work will concern the modification of superalloy compositions as recent results proved their strong influence on the TBC system lifetime, through induced changes in the chemical and mechanical properties of the bond coat ■

Acknowledgements

The authors are grateful to the French Ministry of Defense and the European Commission for partial funding of this work. The authors would like to thank D. BOIVIN, P. JOSSO, S. NAVÉOS, Y. RENOLLET AND C. SANCHEZ for their valuable contributions.

References

[1] M. P. BACOS, J. M. DORVAUX, O. LAVIGNE, R. MEVREL, M. POULAIN, C. RIO, M. H. VIDAL-SETIF - *Performance and Degradation Mechanisms of TBCs for Turbine Blades*. Aerospace Lab 03 - November 2011.
[2] S. ALPÉRINE, M. DERRIEN, Y. JASLIER, R. MÉVREL - *Thermal Barrier Coatings: the Thermal Conductivity Challenge*. AGARD R-823 (1998) 1-1-10.
[3] D.R. CLARKE - *Materials Selection Guidelines for Low Thermal Conductivity Thermal Barrier Coatings*. Surf. Coat. Technol., 163-164 (2003) 67-74.
[4] C.G. LEVI - *Emerging Materials and Processes for Thermal Barrier Systems*. Current Opinion Solid State Mater. Sci., 8 (2004) 77-91.
[5] M. GELL, P.G. KLEMENS - *Thermal Conductivity of Thermal Barrier Coatings*. Mat. Sci. Eng. A, 245 (1997) 143-149
[6] G.E. YOUNGBLOOD, R.W. RICE, R.P. NIGEL - *Thermal Diffusivity of Partially and Fully Stabilized (Yttria) Zirconia Single Crystals.* J. Am. Ceram. Soc., 71 (1988) 255-260.
[7] J.F. BISSON, D. FOURNIER, M. POULAIN, O. LAVIGNE, R. MÉVREL - *Thermal Conductivity of Yttria-Zirconia Single Crystals Determined with Spatially Resolved Infrared Thermography*. J. Am. Ceram. Soc., 71 (2000) 255-260.
[8] M. FÈVRE, A. FINEL, R. CAUDRON, R. MÉVREL - *Local Order and Thermal Conductivity in Yttria-Stabilized Zirconia*. II. *Numerical and expermental investigations of thermal conductivity*. Phys. Rev. B, 72 (2005) 104118-1-7.
[9] B. LECLERCQ, R. MÉVREL - *Thermal Conductivity of Zirconia-Based Ceramics for Thermal Barrier Coatings*. Proc. CIMTEC 2002 , Firenze Italy, July 14-18 (2002).

[10] MC-NG composition [wt. %] : Ni base, 4 Cr, 1 Mo, 5 W, 3.9 Re, 3.8 Ru, 5.8 Al, 0.5 Ti, 5 Ta, 0.1 Si, 0.1 Hf

[10] X. HUANG, D. WANG, M. LAMONTAGNE, C. MOREAU - *Experimental Study of The Thermal Conductivity of Metal Oxides Co-Doped Yttria Stabilized Zirconia.* Mat. Sci. Eng. B, 149 (2008) 63-72.
[11] Y. SHEN, R.M. LECKIE, C.G. LEVI, D.R. CLARKE - *Low Thermal Conductivity Without Oxygen Vacancies in Equimolar $YO_{1.5}+TaO_{2.5}$- and $YbO_{1.5}+TaO_{2.5}$-Stabilized Tetragonal Zirconia Ceramics*. Acta Mater., 58 (2010) 4424-4431.
[12] R. MÉVREL, J.-C. LAIZET, A. AZZOPARDI, B. LECLERCQ, M. POULAIN, O. LAVIGNE, D. DEMANGE - *Thermal Diffusivity and Conductivity of $Zr_{1-x}YxO_{1-x/2}$ (x=0, 0.084 and 0.179) Single Crystals*. J. Europ. Ceram. Soc., 24 (2004) 3081-3089.
[13] M.A. PRÉVOST, R. MÉVREL, M. FÈVRE - *New Ceramic Material for Thermal Barrier Coatings.* Intern. Conf. Europ. Ceram. Soc., Berlin, Germany, June 17-21 (2007).
[14] J. WU, X. WEI, N.P. PADTURE, P. KLEMENS, M. GELL, E. GARCIA, P. MIRANZO, M. OSENDI - *Low-Thermal Conductivity Rare Earth Zirconates for Potential Thermal Barrier Applications*. J. Am. Ceram. Soc., 85 (2003) 3031-3035.
[15] R. VASSEN, X. CAO, F. TIETZ, D. BASU, D. STOVER - *Zirconates as New Materials for Thermal Barrier Coatings*. J. Am. Ceram. Soc., 83 (2000) 2023-2028.
[16] M. V. KRISHNAIAH, P. SRIRAMA MURTHI, C. K. MATHEWS - *Thermal Diffusivity and Thermal Conductivity Studies on Europium, Gadolinium and Lanthanum Pyrohafnates.* Thermochim. Acta, 140 (1989) 103-104.
[17] R. GUO, S. BHALLA, L.E. CROSS - *$Ba(Mg_{1/3}Ta_{2/3})O_3$ Single Crystal Fiber Grown by the Laser Heated Pedestal Growth Technique*. J. Appl. Phys., 75 (1994) 4704-4708.
[18] R. VASSEN, S. SCHWARTZ-LUCKGE, W. JUNGEN, D. STOEVER - US patent 20050260435 A1 (2005).
[19] M.A. PREVOST - *Etude de nouvelles céramiques pour barrière thermique.* PhD Thesis Univ. Paris VI, France (2007).
[20] S. ALPERINE, V. ARNAULT, O. LAVIGNE, R. MEVREL - US patent 6,333,118 (2001).
[21] U. SCHULZ, B. SAINT-RAMOND, O.LAVIGNE, P. MORETTO, A. VANLIESHOUT, A. BÖRGER - *Low Thermal Conductivity Ceramics for Turbine Blade Thermal Barrier Coating Application*. Ceram. Eng. Sci. Proc., 25 (2004) 375-380.
[22] B. LECLERCQ, R. MÉVREL, A. AZZOPARDI, A. MALIÉ, B. SAINT-RAMOND - US patent 7,374,821 (2008).
[23] B. SARUHAN, U. SCHULZ, R. VASSEN, P. BENGTSSON, C. FRIEDRICH, R. KNÖDLER, O. LAVIGNE, P. MORETTO, C. SIRY, F. TARICCO, N COIGNARD, R. WING. - *Evaluation of Two New Thermal Barrier Coating Materials Produced by APS and EB-PVD*. Ceram. Eng. Sci. Proc., 25 (2004) 363-373.
[24] U. SCHULZ, C. LEYENS, K. FRITSCH, M. PETERS, B. SARUHAN-BRINGS, O. LAVIGNE, J.-M. DORVAUX, M. POULAIN, R. MÉVREL, M. CALIEZ - *Some Recent Trends in Research and Technology of Advanced Thermal Barrier Coatings.* Aerospace Sci. Technol., 7 (2003) 73-80.
[25] B. PRÉAUCHAT, S. DRAWIN - *Isothermal and Cycling Properties of Zirconia-Based Thermal Barrier Coatings Deposited by PECVD*. Surf. Coat. Technol., 146-147 (2001) 94-101.
[26] F. CERNUSCHI, S. AHMANIEMI, P. VUORISTO, T. MÄNTYLÄ - *Modelling of Thermal Conductivity of Porous Materials: Application to Thick Thermal Barrier Coatings*. J. Europ. Ceram. Soc., 24 (2004) 2657-2667.
[27] J.M. DORVAUX, O. LAVIGNE, R. MÉVREL, M. POULAIN, Y. RENOLLET, C. RIO - *Modelling the Thermal Conductivity of Thermal Barrier Coatings*. AGARD R-823 (1998) 13-1-10.
[28] M. POULAIN, J.-M. DORVAUX, O. LAVIGNE, R. MÉVREL – *Modelling the Thermal Conductivity of Plasma Sprayed TBCs.* Surface Modification Technol. XIV, ed. T.S. Sudarshan, M. Jeandin, ASM Intern. IOM Commun. Ltd (2001) 495-502.
[29] M. BARTSCH, E.R. FULLER JR, U. SCHULZ, J.M. DORVAUX, O. LAVIGNE, S.A. LANGE - *Simulating Thermal Response of EB-PVD Thermal Barrier Coating Microstructure.* Ceram. Eng. Sci. Proc., 24 (2003) 549-554.
[30] D.R. CLARKE, C.G. LEVI, A.G. EVANS – *Enhanced Zirconia Thermal Barrier Coating Systems*. Proc. IMechE, 220 (2006) 85-92.
[31] A.S. GANDHI, C.G. LEVI - *Surface Diffusion Studies on TBC Materials by Grain Boundary Grooving*. Univ. Santa Barbara, CA (2005) (EU-US Project HIPERCOAT).
[32] W.C. HASZ, M.P. BOROM, C.A. JOHNSON - US Patent 5,660,885 (1997).
[33] W.C. HASZ, M.P. BOROM, C.A. JOHNSON - US Patent 5,871,820 (1999).
[34] W.C. HASZ, M.P. BOROM, C.A. JOHNSON - US Patent n° 6,261,643 (2001).
[35] R. DAROLIA, B.A. NAGARAJ - US Patent 6,720,038 (2004).
[36] W.R. STOWELL, J.T. BEGOVITCH, T.W. RENTZ, G.A. MACMILLAN, J.GREENE, J.A. MURPHY, D.P. IVKOVICH Jr, A.J. SKOOG - US Patent 6,465,090 (2002).
[37] B.A. NAGARAJ, J.L. WILLIAMS and J.F. ACKERMAN - US Patent 6,627,323 B2 (2003).
[38] B.T. HAZEL, M.GORMAN, B.A. NAGARAJ - US Patent 7,666,528 (2010).
[39] B.A. NAGARAJ, J.F. ACKERMAN, W.R. STOWELL, C.P. LEE. - US Patent 6,933,066 (2005).
[40] R. DAROLIA, B.A. NAGARAJ, D.G. KONITZER, M.D. GORMAN, M.FU - US Patent Application 20070160859 (2007).
[41] S. KRÄMER, J. YANG, C. G. LEVI - *Infiltration-Inhibiting Reaction of Gadolinium Zirconate Thermal Barrier Coatings with CMAS Melts.* J. Am. Ceram. Soc., 91 (2008) 576-583.
[42] S. KRÄMER, J. YANG, C.A. JOHNSON, C.G. LEVI - T*hermochemical Interaction of Thermal Barrier Coatings with molten CaO-MgO-Al_2O_3-SiO_2 (CMAS) Deposits*. J. Am. Ceram. Soc., 89 (2006) 3167-3175.
[43] B. PINT - *Experimental Observations in Support of The Dynamic-Segregation Theory to Explain the Reactive-Element Effect*. Oxid. Met., 4 (1996) 1-37.
[44] M.P. BACOS, P. JOSSO, S. NAVÉOS - US patent 7,608,301 (2009).
[45] S. NAVÉOS, G. OBERLAENDER, Y. CADORET, P. JOSSO, M.P. BACOS - *Zirconium Modified Aluminide by a Vapour Pack Cementation Process for Thermal Barrier Applications: Formation Mechanisms and Properties.* Mater. Sci. Forum, 461-464 (2004) 375-382.
[46] S. HAMADI, M.P. BACOS, M. POULAIN, A. SEYEUX, V. MAURICE, P. MARCUS - *Oxidation Resistance of a Zr-Doped Nial Coating Thermochemically Deposited on a Nickel-Based Superalloy*. Surf. Coat. Technol., 204 (2009) 756-760.
[47] P.-Y. THÉRY, M. POULAIN, M. DUPEUX, M. BRACCINI - *Adhesion Energy of a YPSZ EB-PVD Layer in Two Thermal Barrier Coating Systems*. Surf. Coat. Technol., 202 (2007) 648-652.

[48] W.S. WALSTON, J.C. SCHAEFFER, W.H. MURPHY - *A New Type of Microstructural Instability in Superalloys -SRZ.* Superalloys 1996, ed. R.D. Kissinger et al. (Warrendale, PA - TMS, 1996) 9-18.
[49] T. NARITA, K.Z. THOSIN, L. FENGQUN, S. HAYASHI, H. MURAKAMI, B. GLEESON, D. YOUG - *Development of Re-Based Diffusion Barrier Coatings on Nickel Based Superalloys.* Mater. Corrosion, 56 (2005) 923-929.
[50] J.A. HAYNES, Y. ZHANG, K.M. COOLEY, L. WALKER, K.S. REEVES, B.A. PINT - *High-Temperature Diffusion Barriers for Protective Coatings*. Surf. Coat. Technol., 188–189 (2004) 153–157.
[51] M.P. BACOS, P. JOSSO - US patent 7,482,039 (2009).
[52] E. CAVALETTI, S. NAVÉOS, S. MERCIER, P. JOSSO, M.P. BACOS, D. MONCEAU - *Ni–W Diffusion Barrier: Its Influence on the Oxidation Behaviour of a β-(Ni,Pt)Al Coated Fourth Generation Nickel-Base Superalloy.* Surf. Coat. Technol., 204 (2009) 761-765.
[53] E. CAVALETTI, S. MERCIER, D. BOIVIN, M.P. BACOS, P. JOSSO, D. MONCEAU - *Development of a NiW in-situ Diffusion Barrier on a Fourth Generation Nickel-Base Superalloy*. Mater. Sci. Forum, 595-598 (2008) 23-32.
[54] D. POQUILLON, D. MONCEAU - *Application of a Simple Statistical Spalling Model for the Analysis of High-Temperature. Cyclic oxidation kinetic data.* Oxidation Metals, 59 (2003) 409-431.
[55] E. CAVALETTI - *Etude et développement de nouveaux revêtements avec barrières de diffusion pour application sur aubes de turbines à gaz en superalliage à base de nickel*. PhD Thesis, Univ. Toulouse, France (2009).

Acronyms

TBC (Thermal Barrier Coating)
8YPSZ (8 wt.% Yttria Partially Stabilized Zirconia)
20YFSZ (20 wt.% Yttria Fully Stabilized Zirconia)
CMAS (Calcium-Magnesium-Alumino-Silicates)
EB-PVD (Electron Beam-Physical Vapor Deposition)
PE-CVD (Plasma Enhanced Chemical Vapor Deposition)
K (Thermal Conductivity)
FDM (Finite Difference Method)
FEM (Finite Element Method)
FIB (Focused Ion Beam)
AFM (Atomic Force Microscopy)
GDMS (Glow Discharge Mass Spectroscopy)
ToF-SIMS (Time-of-flight Secondary Ion Mass Spectroscopy)
TCP (Topological Compact Phase)
TGO (Thermally Grown Oxide)
SRZ (Secondary Reaction Zones)
DB (Diffusion Barrier)
SEM (Scanning Electron Microscopy)
BSE (Back Scattered Electron)
EDS (Energy Dispersive Spectroscopy)
XRD (X-Ray Diffraction)
EBSD (Electron Back Scattered Diffraction)

AUTHORS

Marie-Pierre Bacos graduated from the Ecole Nationale Supérieure de Chimie in Paris (1981) and received a PhD degree in Applied Chemistry from University of Paris VI (1983). She joined Onera in 1983 where she has been involved in oxidation and corrosion mechanisms and in the development of innovating coatings and brazing technologies. She is the Head of the Materials and Architecture Research Unit at Onera Châtillon.

Jean-Marc Dorvaux joined the Material Department of Onera as a research scientist in thermal physics. His activities cover both the experimental development of testing and the modelling of heat transfer in materials in harsh environments.

Stéphane Landais graduated as a materials science engineer from the Conservatoire National des Arts et Métiers in Paris. He joined Onera in 1991 to participate in the development of new ceramic composites. Since 1998, he is in charge of PVD and CVD coating laboratory at Onera-Palaiseau.

Odile Lavigne graduated as a physicist engineer from the Ecole Supérieure de Physique et Chimie Industrielles in Paris and obtained a PhD degree in Material Science from the University of Paris VI. She joined Onera in 1986, where she was successively involved in developing stealth systems and high temperature composite materials for space applications. For the past fifteen years she has been working as a senior scientist on thermal barrier systems for gas turbine engines.

Rémy Mévrel has a long experience in the field of high temperature protective coatings. His activities combine experimental and theoretical studies, in relation with both academic scientists and industrial partners. He introduced research activities on thermal barrier coatings at Onera in the early 80s and has become rapidly a world known expert in this field.

Martine Poulain has been working at Onera since 1979, initially in the "Materials" department. She was involved in the development of protective coatings and she received her PhD degree from the University of Paris XI in 1999, on the topic of thermal insulation capabilities of TBCs. Her present research themes in the Metallic Materials and Structure department focus on the damage and life modeling of TBCs, and the coating by design approach.

Catherine Rio graduated from the Institut Universitaire de Technologie of Paris XI. She has been working at Onera since 1982 as a specialist in physical measurements, metallography and microstructure characterization on a wide range of high temperature materials and coatings.

Marie-Hélène Vidal-Sétif graduated as a chemical engineer from the Ecole Supérieure de Physique et Chimie Industrielles in Paris and obtained a PhD degree in Physical Chemistry from the University of Paris XI. She joined Onera in 1987, where she was successively involved in the development of metal matrix composites (MMC), corrosion behavior of MMC and aluminum alloys. For the past 7 years she has been working as a senior scientist on thermal barrier systems for gas turbine engines.